Applied Radiation and Isotopes 215 (2025) 111580

Contents lists available at ScienceDirect

Applied Radiation and Isotopes

journal homepage: www.elsevier.com/locate/apradiso

Production of ^{43}Sc and ^{44g}Sc from natural CaF_2 material using an FN Tandem accelerator

Austin D. Nelson *, Adam M. Clark, Thomas L. Bailey, Lauren K. Callahan, Philippe Collon

Department of Physics, University of Notre Dame, Notre Dame, IN, 46556, United States

ARTICLE INFO

Keywords:
^{43}Sc ^{44g}Sc
Activation
Thick target yield

ABSTRACT

The radioisotopes of ^{43}Sc and ^{44}Sc are promising in the field of theranostics for their role as β^+ emitters in theranostic pairs with ^{47}Sc. Production of these isotopes through various nuclear reactions using either cyclotrons or linear accelerators is of particular interest and previous studies have provided results using accelerated beams of protons, deuterons, and alpha particles. A novel production technique, using an ion source cathode packed with natural calcium fluoride material and irradiated with a ^{3}He beam, was tested at the Nuclear Science Laboratory at the University of Notre Dame in order to initially study the production of ^{41}Ca. Gamma-ray spectrometry revealed presence of ^{43}Sc and ^{44}Sc in the target, and allowed for the first measurement of their yield due to reactions of ^{3}He on natural calcium. The calculated thick target yields of ^{43}Sc and ^{44g}Sc from the reactions ^{nat}Ca(^{3}He,x)^{43}Sc and ^{nat}Ca(^{3}He,x)^{44g}Sc are compared to theoretical results using TALYS cross section models. Overall, results agree well with models at lower beam energies but tend to diverge at higher energies.

1. Introduction

Theranostics is the integration of both therapeutics and diagnostics, used for the detection and treatment of various tumors (Burkett et al., 2023). The technique is based on using the same targeting molecule (or vector in general) labelled with either a diagnostic or therapeutic emitter; therefore an identical, or at least strongly similar, chemical entity is required. The most promising way to do this is through theranostic pairs; a pair of isotopes, preferably of the same element but not exclusively, where one isotope is a β^+ emitter used for Positron Emission Tomography (PET) imaging and the other is a β^- emitter used for radiation therapy (Carzaniga et al., 2017, 2019). Some of the most promising pairs currently include ^{64}Cu/^{67}Cu, ^{43}Sc/^{47}Sc, and ^{44g}Sc/^{47}Sc.

Since ^{43}Sc and ^{44g}Sc are both β^+ emitters, they are both relevant for the PET imaging side of theranostics. Previously, this was dominated by ^{18}F and, more recently ^{68}Ga, but using scandium has the potential to be more effective due to its physical and chemical properties (Carzaniga et al., 2017; Sitarz et al., 2018). The half-lives of ^{43}Sc ($t_{1/2}$ = 3.891 h (Singh and Chen, 2015)) and ^{44g}Sc ($t_{1/2}$ = 3.97 h (Chen et al., 2011)) are both significantly longer than that of ^{18}F ($t_{1/2}$ = 1.83 h (Tilley and Cheves, 1995)) and ^{68}Ga ($t_{1/2}$ = 1.13 h (Mccutchan, 2012)), allowing for advantages in production and distribution of the radioisotope. ^{43}Sc decays with a similarly high total positron yield as ^{68}Ga (~88%), but with positrons that have much lower mean energies (476 keV (Singh and Chen, 2015)) compared to ^{68}Ga (829.5 keV (Mccutchan, 2012)). Combined with the associated low energy gamma-ray (372.9 keV) that also has a low intensity (22.5%), this means less of a dose would be given to a patient. ^{44g}Sc, on the other hand, decays with a high positron yield (94.3%) with a mean positron energy of 630.2 keV, and has an associated high energy gamma-ray (1157.0 keV) with a high branching ratio (99.9%) (Chen et al., 2011), which makes it an excellent candidate for γ-coincidence imaging but could also increase the radiation dose to a patient. However, this could be alleviated with shorter measurement times or similar measurements using lower activities by utilizing the three-photon technique (Carzaniga et al., 2019; Sitarz et al., 2018). The other issue with ^{44g}Sc is the co-production of the long-lived metastable state ^{44m}Sc ($t_{1/2}$ = 58.6 h (Chen et al., 2011)) that cannot be chemically separated from the ground state.

The process of creating ^{43,44g}Sc from proton, deuteron, and alpha beams incident on a variety of natural or enriched calcium targets has been studied extensively recently (Carzaniga et al., 2017, 2019; Sitarz et al., 2018; Severin et al., 2012; Alabyad et al., 2018). The data provided within this paper are a rather unexpected result from an experiment performed to study a novel activation process for the production of ^{41}Ca (Nelson et al., 2022). Through the analysis of the gamma-ray spectrometry data from that experiment, it was found that there were

* Corresponding author.
E-mail address: anelso12@alumni.nd.edu (A.D. Nelson).

https://doi.org/10.1016/j.apradiso.2024.111580
Received 16 January 2024; Received in revised form 14 October 2024; Accepted 5 November 2024
Available online 6 November 2024

two gamma-ray peaks that resulted from the ^{3}He beam interacting with the calcium material. These peaks were at energies of 372.9 keV and 1157.0 keV and were identified as being from the decay of ^{43}Sc and ^{44g}Sc, respectively. Due to the promising nature of these isotopes in the field of theranostics, we present the first known results of their production using a ^{3}He beam on a natural calcium target.

2. Materials and methods

2.1. Experimental setup

For the experiment, a novel setup was designed to activate CaF_2 powder in a SNICS ion source cathode to initially study the production of ^{41}Ca. Details on the complete setup and relevant pictures are given in (Nelson et al., 2022), but a short summary will be given here. To hold the cathodes directly in the way of the beam, three separate cathode holders were designed and machined to be attached to a target ladder. The main parts of the cathode holders were made of polyester plastic for insulating purposes. A tantalum shield was placed in front of each cathode holder with a 1 mm hole drilled in the center to act as a collimator. This hole was precisely positioned to be in line with the opening of the cathode in order to maximize hitting beam on the cathode material. An isolated thin, metal washer was placed between the tantalum opening and the cathode, and a suppression voltage of −300 V was able to be applied to the washer via a short metal screw. Suppression was necessary to avoid any escaping secondary electrons ejected by the beam from impinging on the cathode, and thus distorting the beam current measurement incident on the target. The copper cathode with the CaF_2 powder was positioned at the end of the holder, embedded within the plastic to isolate it from all other pieces, and fastened via two small screws, which were also used to collect the charge from the cathode when bombarded by the beam. Both the suppression and cathode screws were attached by separate wire cables and sent to individual BNC feedthroughs.

All cathodes used for this experiment were made from vacuum-cleaned, high-purity Cu and purchased from National Electrostatics Corp. (NEC). Each cathode was initially weighed before being packed with CaF_2 powder, purchased from Alfa Aesar (99% purity). All tools used to pack the powder were cleaned beforehand with ethanol and deionized water and baked in a vacuum oven at 120 °C for 2 h to prevent any contamination. After packing, cathodes were weighed again to determine the amount of $^{nat}CaF_2$ powder and then sealed in the back with a small piece of Cu wire. The dimensions of the target were then just the internal dimensions of the packed cathode, 1 mm in diameter and 3.5 mm in length. Using the mass of the packed CaF_2 powder and these internal dimensions of the cathode, the density for each packed cathode was calculated, with an overall average density of around 3.0 ± 0.2 g/cm^3.

For the irradiations, a small scattering chamber was set up and aligned to the existing beamline. The chamber had five equidistant openings at 45-degree increments around the outside, an opaque bottom plate, and a solid aluminum lid on top. A target ladder was connected to a hand-driven linear motion device and attached to the scattering chamber at an opening situated 90° from the beam entrance point. Attached to the target ladder were three cathode holders, along with a small Faraday cup for beam tuning. Two blank-off pieces with three BNC feed-through connections each provided current outputs for all three cathodes, current output readings of the Faraday cup and target ladder, and a suppression voltage.

A 2-inch quartz viewer was attached at the back end of the scattering chamber in order to ensure alignment of the beam and cathode. The position of the cathode was able to be viewed with a scope on the beamline, originally used to set up the chamber. Small adjustments could then be made by hand with the linear motion device to align each cathode with beam center before each irradiation.

2.2. Irradiations

Irradiations of the target material were performed at the Nuclear Science Laboratory (NSL) at the University of Notre Dame. Negative helium ions were created in a duoplasmatron ion source and accelerated using the 10 MV FN Tandem accelerator. The 2+ charge state was then selected by the analyzing magnet and the beam was sent down the +15-degree beamline to the experimental setup, as described above. Each irradiation was performed at a specific beam energy, as determined by the FN terminal voltage (±20 kV) and NMR-calibrated magnetic field in the analyzing magnet, with values given in Table I. It should be noted that Sample 1 was used purely as a test of the setup with an α beam.

The irradiations were performed over two separate days, with Samples 1–14 being activated on one day and Samples 15–24 being activated on another, with both following the same procedure. The highest energy beam was selected first, and each subsequent lower energy was found by scaling the terminal voltage of the accelerator and the magnets of the system until the appropriate energy was obtained. At each energy, the beam was tuned to the Faraday cup attached to the target ladder by maximizing the amount of current on the cup and minimizing the current on the ladder, thereby attaining the narrowest beam possible. Once the beam was tuned, the target cathode was moved into place by adjusting the target ladder and centered using the scope and quartz viewer behind the setup. The cathode was then irradiated for a predetermined amount of time based on the incoming beam current and cross section models. The amount of beam on target was monitored continuously while the collected charge was integrated and digitized, with the total values for each energy shown in Table 1.

2.3. Gamma-ray measurements

After each activation had concluded, the irradiated cathode was placed in an off-line counting station as soon as possible in order to measure the activity of decaying isotopes produced during the activation process. Activity measurements were performed with a large volume, closed-end coaxial HPGe Canberra detector (Model: GC3518). The cathodes were positioned on a specially designed holder, shown in Fig. 1, and placed inside a four-inch-thick lead brick castle lined inside with an oxygen-free copper layer to minimize background. The holder was machined out of pieces of aluminum and designed for height

Table 1
Irradiation parameters for all activated samples.

Sample Number	Beam Energy [MeV]	Charge Collected [nC]	Irradiation Time [s]
1	24.54	7256.5	1800
2	25.22	1213.3	480
3	25.22	1218.3	480
4	23.74	1153.7	780
5	22.25	1126.5	660
6	20.82	1160.7	300
7	19.35	1128.6	240
8	17.88	1173.9	420
9	16.43	1282.9	360
10	14.88	1499.9	1140
11	13.46	1779.9	1200
12	11.97	2460.4	960
13	10.50	3660.1	1860
14	9.00	7766.6	4680
15	25.22	1837.0	360
16	23.62	1723.9	430
17	22.53	1671.3	330
18	21.05	1678.3	410
19	19.56	1696.0	330
20	18.09	1750.4	430
21	16.63	1897.4	625
22	15.12	2156.1	713
23	13.64	2632.8	870
24	12.05	3542.7	700

Fig. 1. Cathode holder designed for use in the gamma counting station. The cathode sits in the grove, facing outward and the stand can be adjusted by loosening the two set screws and moving the top piece up or down.

adjustment to center on the detector head. A groove was fashioned toward the edge of the holder to make the face of the cathode lie flat with the edge of the stand and completely parallel to the face of the detector. Before the activations took place, the detector was calibrated for both energy and efficiency using calibration sources of ^{22}Na, ^{60}Co, ^{133}Ba, and ^{152}Eu, all with known activities.

Each cathode was placed in the counting station at 9.5 cm from the detector head, for two, 15-min acquisitions as soon as possible after the end of beam time, with the time between the end of irradiation and the start of the counting sequence being recorded. Acquisitions were also taken 48 h later, with the same 15-min live time, to observe any longer-lived isotopes and account for any background corrections. Any dead-time losses during acquisition were small, typically between 10 and 60 s, and the number of counts was corrected for using the live-time of the detector, with activity calculations also being corrected for the time elapsed from the end of the irradiation process.

3. Results

A representative gamma-ray spectrum is shown in Fig. 2 and depicts the detected gamma-ray lines from the two scandium isotopes of interest, along with several other prominent isotopes. It should be noted that the ^{137}Cs peak was from a contaminated lead brick in the surrounding lead castle and was seen on all calibration and sample spectra. The initial activity for each isotope can be calculated using

$$A_0 = \frac{N_\gamma}{\epsilon(E_\gamma)\cdot I_\gamma \cdot t_L}\cdot\frac{\lambda\cdot t_m\cdot e^{\lambda t_C}}{(1-e^{-\lambda t_m})} \tag{1}$$

where N_γ is the net peak area, λ is the isotope's decay constant, $\epsilon(E_\gamma)$ is

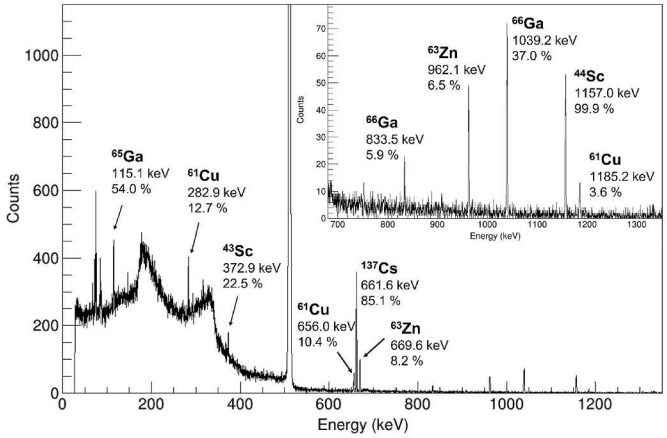

Fig. 2. Representative gamma-ray spectrum for an irradiated cathode (Sample 3 in this case). There are several radionuclides produced from the irradiation of the Cu cathode and a few Sc isotopes seen from the production of ^{3}He on ^{nat}Ca.

the efficiency of the detector at the specific energy of the gamma-ray line, I_γ is the gamma-ray intensity, t_L is the live time of the data aquisition, t_C is cooling time elapsed between the end of irradiation and start of the measurement, and t_m is the real measurement time of the data acquisition. The attenuation of gamma rays due to the material thickness was investigated using the NIST-XCOM database. At the highest beam energy used for irradiation (25.5 MeV), the beam is only able to travel a maximum of around 0.3 mm into the material, with the total material thickness being around 3.5 mm. Calculations were made using this maximum position with the calculated values for the transmission of the ^{43}Sc line (372.9 keV) being around 99.1% and the transmission for the ^{44g}Sc line (1157 keV) being around 99.5%. Therefore, no correction to the net peak area was necessary for these slight attenuation factors.

The total yield can then be found by using the calculated initial activity and the total charge collected on the cathode material Q, using

$$Y = \frac{\lambda A_0}{\frac{Q}{t_i}(1-e^{-\lambda t_i})} \tag{2}$$

where t_i is the irradiation time.

In order to compare to theoretical models, the predicted number of particles created through the reaction of interest can be calculated using a similar approach taken in (Nelson et al., 2022). However, when it comes to medical isotope production, it is often more useful to express the results in terms of yield with units of MBq/μAh. Therefore, the yield of each Sc isotope can be calculated using the following equation:

$$Y_{Sc} = \frac{\rho_{CaF2}\cdot N_A\cdot\lambda}{M_{CaF2}}\cdot\sum_n a_n\int_{E_0}^{E_{beam}}\frac{\sigma_n(E)}{-\frac{dE}{dx}(E)}dE \tag{3}$$

where ρ_{CaF2} is the measured density of the CaF_2 powder packed in the sample, N_A (=6.022 × 10 ^{23} mol^{-1}) is Avogadro's constant, λ is the isotope's decay constant, and M_{CaF2} (=78.07 g/mol) is the molar mass of CaF_2. The sum considers all stable calcium isotopes, their abundance a_n, and is integrated over the cross section of the various reaction channels $\sigma_n(E)$ within the material stopping power dE/dx(E) over the range of possible energies.

3.1. ^{43}Sc production

^{43}Sc is formed in several reaction channels of ^{3}He-induced nuclear reactions on all the isotopes present in natural calcium. Their predicted excitation functions were obtained using TALYS-1.8 using default parameters and are shown in Fig. 3. They were used as an input to Equation (3). As can be seen, the dominant pathways are through the various

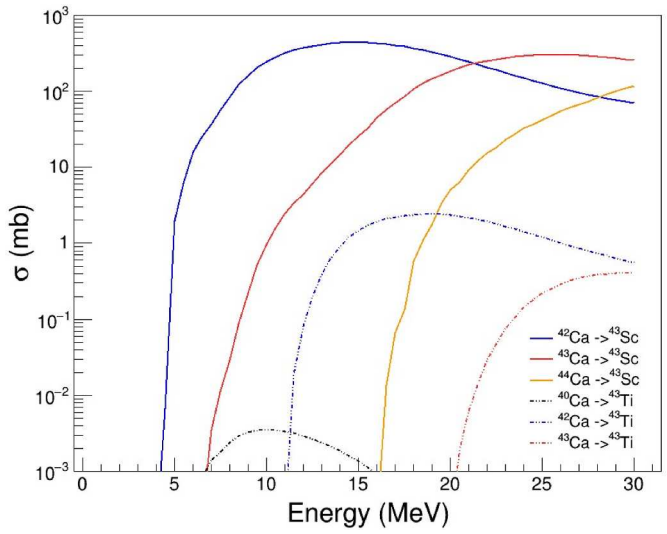

Fig. 3. TALYS-1.8 predicted cross sections for the production of ^{43}Sc from the interaction of ^{3}He with the various natural Ca isotopes.

calcium isotopes (^{42,43,44}Ca) directly, with minor contributions through the production of ^{43}Ti, which subsequently decays to ^{43}Sc through electron capture with a very short half-life of 509 ms (Singh and Chen, 2015). Each TALYS curve was fitted with a fifth-to-seventh order polynomial function, chosen based on the reduced chi squared values. The stopping power data was calculated using SRIM-2013 (Ziegler and Biersack, 2010) and fit with a power function over the energy range of interest using ROOT. The predicted yield was then calculated by integrating all the various reaction channels and summing over the different isotopic abundances of the material with results given in Table II.

To calculate the measured yield of ^{43}Sc, each irradiated sample's gamma-ray spectrum was analyzed to determine the activity of ^{43}Sc using its dominant peak at 372.9 keV. The initial activity was calculated using Equation (1). Here, the number of counts in the peak was calculated from the fit of the peak using ROOT, the efficiency was calculated using the efficiency curve from the known calibration isotopes, and the gamma-ray intensity I_γ and decay constant ($\lambda = \ln(2)/t_{1/2}$) were found on Brookhaven National Laboratory's National Nuclear Data Center (NNDC) to be 22.5% and 0.178 h^{-1}, respectively (Singh and Chen, 2015). Both the measurement time t_m and cooling time passed since the end of the irradiation process t_C were also known for each acquisition. The yield was then calculated using Equation (2).

These calculations were performed on all samples for both rounds of activations at all activated energies. Table 2 shows the results of the measured initial activities, the measured yields, and the predicted yields using the cross-section data from TALYS. These data were all plotted as a function of the beam energy of the activation, with the results shown in Fig. 4. Results for samples 11–14 are not given as there were no discernible counts in the peak above background. Error bars on the measured data points were the result of the propagation of uncertainties due to Poisson statistics in the number of counts in the peak, uncertainties in the efficiency of the detector, the given uncertainties of λ and I_γ from NNDC, a 5% uncertainty on the collected charge from the beam current, and uncertainties in the recording times. The region of uncertainty in the predicted yield calculations are the result of the

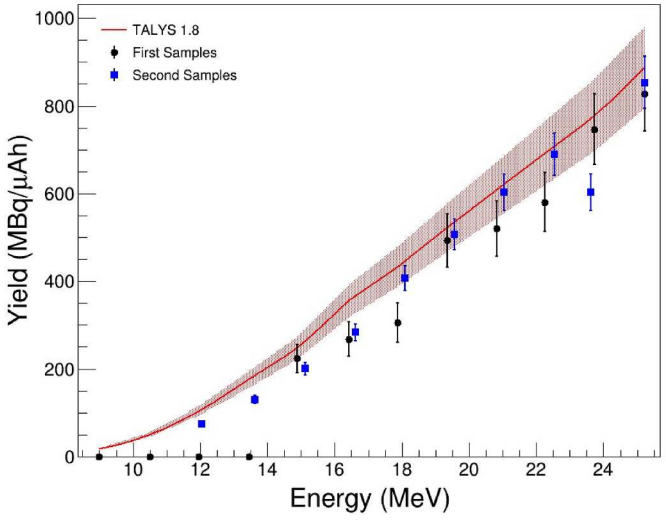

Fig. 4. Results on the production of ^{43}Sc. The predicted yield is shown by the red curve and associated uncertainty in the red region and the measured values from the activated samples shown as black and blue points with their associated uncertainties. (For interpretation of the references to colour in this figure legend, the reader is referred to the web version of this article.)

Table 2
^{43}Sc and ^{44}Sc calculated activities and yield results.

Sample Number	Beam Energy [MeV]	Measured ^{43}Sc Activity [Bq]	Measured ^{43}Sc Yield [MBq/μAh]	Predicted ^{43}Sc Yield [MBq/μAh]	Measured ^{44g}Sc Activity [Bq]	Measured ^{44g}Sc Yield [MBq/μAh]	Predicted ^{44g}Sc Yield [MBq/μAh]
3	25.22	277(*26*)	828(*86*)	890(*93*)	168(*15*)	502(*51*)	487(*52*)
4	23.74	235(*23*)	747(*81*)	780(*82*)	126(*13*)	401(*44*)	461(*51*)
5	22.25	179(*19*)	580(*67*)	693(*73*)	67(*9*)	218(*29*)	395(*44*)
6	20.82	167(*19*)	520(*63*)	610(*64*)	55(*8*)	173(*26*)	301(*34*)
7	19.35	154(*18*)	493(*61*)	524(*55*)	55(*8*)	178(*26*)	218(*25*)
8	17.88	98(*14*)	305(*45*)	434(*46*)	44(*7*)	138(*22*)	156(*18*)
9	16.43	95(*13*)	268(*40*)	356(*37*)	35(*6*)	98(*17*)	119(*14*)
10	14.88	91(*13*)	224(*33*)	249(*26*)	29(*5*)	72(*13*)	83(*10*)
11	13.46	–	–	178(*19*)	26(*5*)	55(*11*)	64(*8*)
12	11.97	–	–	105(*11*)	30(*5*)	45(*8*)	43(*5*)
13	10.50	–	–	51(*5*)	24(*5*)	25(*5*)	26(*3*)
14	9.00	–	–	18(*2*)	27(*5*)	14(*2*)	13(*2*)
15	25.22	420(*21*)	853(*59*)	890(*93*)	185(*9*)	372(*26*)	487(*52*)
16	23.62	282(*14*)	603(*42*)	780(*82*)	145(*7*)	307(*22*)	461(*51*)
17	22.53	316(*16*)	690(*48*)	707(*74*)	117(*6*)	254(*18*)	408(*45*)
18	21.05	271(*13*)	603(*42*)	624(*65*)	99(*5*)	218(*15*)	315(*36*)
19	19.56	231(*12*)	507(*35*)	539(*56*)	64(*3*)	139(*10*)	229(*26*)
20	18.09	193(*10*)	407(*28*)	450(*47*)	55(*3*)	116(*8*)	164(*19*)
21	16.63	145(*7*)	283(*20*)	364(*38*)	50(*3*)	96(*7*)	122(*14*)
22	15.12	116(*6*)	200(*14*)	271(*28*)	38(*2*)	64(*5*)	90(10)
23	13.64	90(*5*)	130(*9*)	184(*19*)	37(*2*)	53(*4*)	65(*8*)
24	12.05	69(*4*)	75(*5*)	105(*11*)	35(*2*)	36(*3*)	43(*5*)

propagation of uncertainties in the mass and density of the material, the given uncertainty in λ from NNDC, and the uncertainties in the fits for the cross section and stopping power for the various reaction channels.

3.2. ^{44g}Sc production

Using a similar approach as described for the ^{43}Sc production, the predicted production of ^{44g}Sc was also determined using Equation (3) above, with the only differing variable being the cross section through the different reaction channels of the reaction ^{nat}Ca(^{3}He,x)^{44g}Sc. The cross-section predictions were also performed using TALYS-1.8 with default parameters for the various pathways of production for ^{44}Sc, with the predicted results shown in Fig. 5. Included in the plot are the cross-section predictions for the production of ^{44m}Sc through the various reactions with the isotopes of calcium. Similarly, each TALYS curve was fit with a fifth-to-seventh order polynomial function, chosen based on the reduced chi squared values. The stopping power data was calculated using SRIM-2013 and fit with a power function over the energy range of interest using ROOT. The predicted yield was then calculated by integrating all the various reaction channels and summing over the different isotopic abundances of the material with results given in Table 2.

The measured yield of ^{44g}Sc was calculated in a similar manner to that of ^{43}Sc above, but this time using its characteristic peak at 1157.0 keV. This process was performed on all samples for both rounds of activations at all activated energies. Due to the rather serendipitous nature of the experimental data, the contribution to the yield from the decay of ^{44m}Sc was not able to be separated from the direct production data since the gamma-ray spectrometry acquisitions were too short to notice a peak in the spectrum. Thus, the decay of ^{44m}Sc is included in the yield calculations for completeness, however, it is only expected to have a minor contribution to the overall yield due to its longer half-life and much lower predicted cross sections (see Fig. 5).

Table 2 shows the results of the measured initial activities, the measured yield, and the predicted yield using the cross-section data from TALYS. The comparison between the calculated and predicted yields as a function of beam energy is shown in Fig. 6. Error bars in both the measured data points and predicted yield region were calculated in a similar way as those described above for ^{43}Sc.

4. Discussion

The results from all samples over the energy range of 9.0–25.5 MeV show mixed agreement with the theoretical predicted results from TALYS. For the first set of ^{43}Sc and ^{44g}Sc measurements, statistics for the number of counts in the peaks were relatively low, which led to much larger error bars on the measurements. The second set of measurements on ^{43}Sc have better statistics and still tend to agree with TALYS predictions. However, there does seem to be a slight difference in the yield curve between the measured and predicted values at the lower energy points where TALYS seems to over-predict compared to the measured results. This could mean that the cross sections through the pathways of ^{42}Ca or ^{43}Ca are a bit over-represented, as they are the two dominant pathways at the lower energies between 12 and 18 MeV. A dedicated experiment using higher beam intensities and enriched calcium targets could enhance the production of ^{43}Sc through this method, but would need to be verified.

A plot comparing the experimental yields for ^{43}Sc of the data presented in this paper to previously published reports is shown in Fig. 7. Included are data points from reactions using proton, deuteron, and

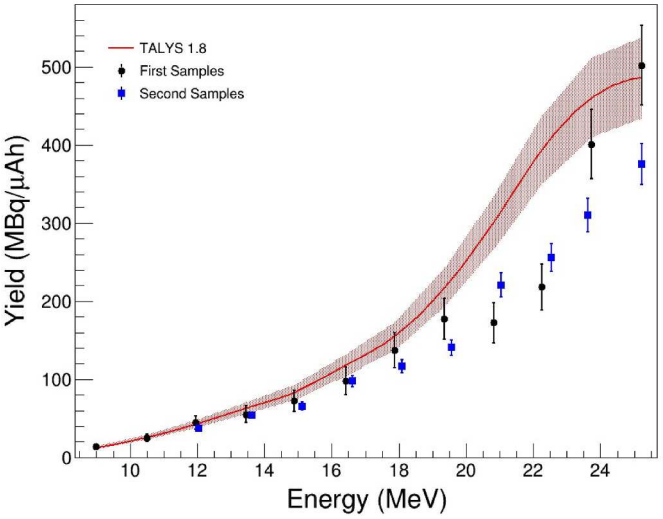

Fig. 6. Results on the production of ^{44g}Sc. The predicted yield is shown by the red curve and associated uncertainty in the red region and the measured values from the activated samples shown as black and blue points with their associated uncertainties. (For interpretation of the references to colour in this figure legend, the reader is referred to the web version of this article.)

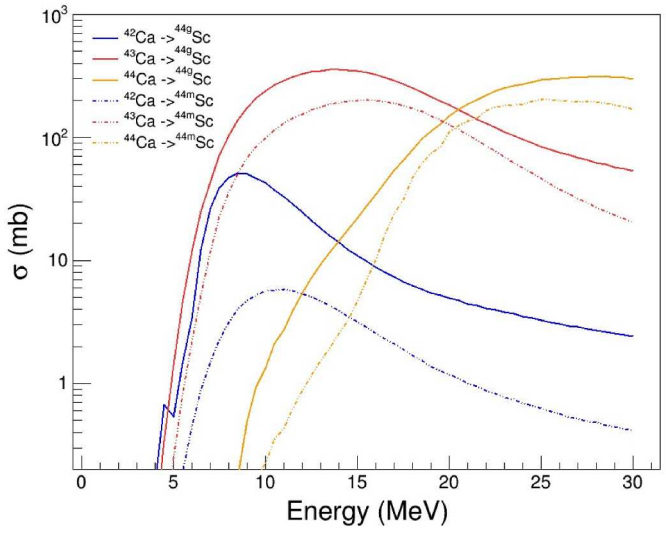

Fig. 5. TALYS-1.8 predicted cross sections for the production of ^{44g}Sc and ^{44m}Sc from the interaction of ^{3}He with the various natural Ca isotopes.

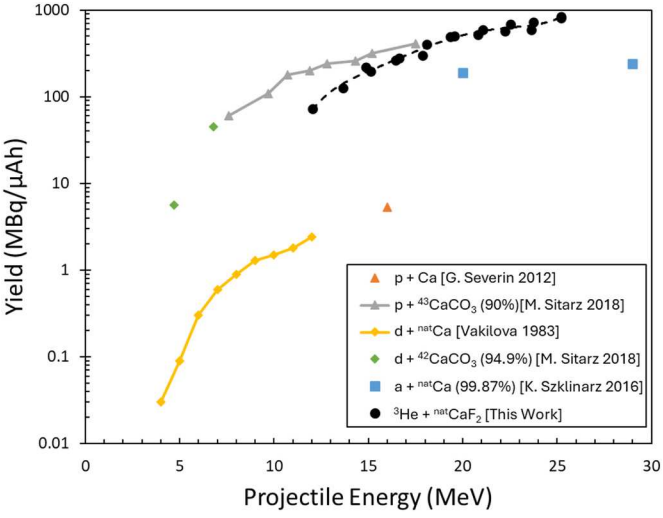

Fig. 7. Combined results for the production of ^{43}Sc, including a comparison of the results of this work to previously published studies involving various reaction pathways (Sitarz et al., 2018; Severin et al., 2012; Szkliniarz et al., 2016; Vakilova et al., 1983).

alpha beams at various projectile energies. Data was provided by the EXFOR database for the reactions of interest. As can be seen, the yield of ^{43}Sc from the reaction ^{3}He + $^{nat}CaF_2$ presented in this paper tends to dominate at projectile energies greater than 18 MeV. Despite the higher beam energy, the yields are comparable and even surpass those of the reaction p + $^{43}CaCO_3$ (Sitarz et al., 2018) without the need for an enriched target, thus highlighting the usefulness of this particular reaction and technique.

For ^{44g}Sc, the measured results tend to show a discrepancy with the theoretical values as the energy starts to increase above a beam energy of 18 MeV. Particularly in the second round of samples, there seems to be an over-prediction by TALYS in the range of 18–25 MeV, suggesting that the cross section may increase quicker and possibly peak at a lower energy than predicted. However, the production of ^{44g}Sc is also dependent on three different reactions from the isotopes of calcium, with the contributions from ^{42}Ca and ^{43}Ca tailing off in this energy range and the cross section for ^{44}Ca starting to build up. Therefore, it is also possible that the cross section for ^{42,43}Ca doesn't fall as quickly as TALYS claims, or that ^{44}Ca builds up quicker than expected, or some combination of these scenarios. A study of the different reactions using various enriched isotopes could confirm which of these statements to be true if these results are useful and desired in the ever-growing field of medical isotope production.

A comparison of the yield results for the production of ^{44g}Sc from this paper to those from other experimental results is shown in Fig. 8. Included are data points from reactions using proton and deuteron beams at various projectile energies. Data was provided by the EXFOR database (Zerkin and Pritychenko, 2018; Otuka et al., 2014) for the reactions of interest. The production of ^{44g}Sc from the reaction ^{3}He + $^{nat}CaF_2$ in this work outperforms the other reaction that uses a natural target (p + $^{nat}CaCO_3$ (Carzaniga et al., 2019)) by a factor of up to 20 × but is around 3 × less productive than the same reaction using an enriched $^{44}CaCO_3$ target. Since the enrichment of the target can significantly improve the production yields, a similar enrichment of a CaF_2 target with a ^{3}He beam could also outperform that of the reaction in (Sitarz et al., 2018), thereby providing an even greater contribution to ^{44g}Sc production. Further experimental results would be needed to ultimately determine how significant this impact is by a more direct comparison of the two different reactions. However, this reaction is not without its drawbacks, particularly that of the rare availability and cost of ^{3}He. It should also be noted that there is the simultaneous production of ^{44m}Sc that comes from these reactions that cannot be chemically separated from ^{44g}Sc in the samples.

Overall, the results from this study on the production of ^{43,44g}Sc using a ^{3}He beam on $^{nat}CaF_2$ material tends to show good agreement with theoretical models, but results tend to diverge at higher beam energies. While there have been several recent studies on the production of ^{43,44g}Sc using proton, deuteron, and alpha beams (Carzaniga et al., 2017, 2019; Sitarz et al., 2018; Severin et al., 2012; Alabyad et al., 2018), this is the first known result of the production of these isotopes using a ^{3}He beam and a natural powder target, allowing for an easy experimental setup and quick activation results. With much higher beam intensities and using enriched targets, the process could easily produce these isotopes in abundance for any pre-clinical medical applications that may desire them.

CRediT authorship contribution statement

Austin D. Nelson: Writing – original draft, Formal analysis, Data curation, Conceptualization. **Adam M. Clark:** Writing – review & editing, Conceptualization. **Thomas L. Bailey:** Writing – review & editing, Conceptualization. **Lauren K. Callahan:** Writing – review & editing, Conceptualization. **Philippe Collon:** Writing – review & editing, Supervision, Project administration, Funding acquisition, Conceptualization.

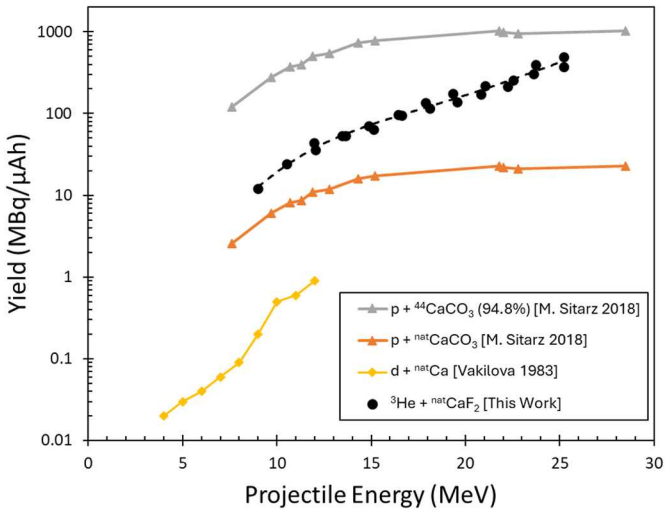

Fig. 8. Combined results for the production of ^{44g}Sc, including a comparison of the results of this work to previously published studies involving various reaction pathways (Sitarz et al., 2018; Vakilova et al., 1983).

Declaration of competing interest

The authors declare the following financial interests/personal relationships which may be considered as potential competing interests: Austin Nelson reports financial support was provided by National Science Foundation. Adam Clark reports financial support was provided by National Science Foundation. Thomas Bailey reports financial support was provided by National Science Foundation. Lauren Callahan reports financial support was provided by National Science Foundation. Philippe Collon reports financial support was provided by National Science Foundation. If there are other authors, they declare that they have no known competing financial interests or personal relationships that could have appeared to influence the work reported in this paper.

Acknowledgements

We would like to thank Graham Peaslee and Anthony (Tony) Miller for providing their insight through various discussions regarding this work. This work is supported by the National Science Foundation under grant numbers PHY-2011890 and PHY-2310059.

Data availability

Data will be made available on request.

References

Alabyad, M., Mohamed, G.Y., Hassan, H.E., Tak acs, S., Ditr oi, F., 2018. Experimental measurements and theoretical calculations for proton, deuteron and particle induced nuclear reactions on calcium: special relevance to the production of 43,44Sc. J. Radioanal. Nucl. Chem. 316, 119–128. https://doi.org/10.1007/s10967-018-5733-4.

Burkett, B.J., Bartlett, D.J., McGarrah, P.W., Lewis, A.R., Johnson, D.R., Berberoğlu, K., Pandey, M.K., Packard, A.T., Halfdanarson, T.R., Hruska, C.B., Johnson, G.B., Kendi, A.T., 2023. A review of theranostics: perspectives on emerging approaches and clinical advancements. Radiol Imaging Cancer 5 (4), e220157. https://doi.org/10.1148/rycan.220157.

Carzaniga, T.S., Auger, M., Braccini, S., Bunka, M., Ereditato, A., Nesteruk, K.P., Scampoli, P., Turler, A., van der Meulen, N., 2017. Measurement of 43Sc and 44Sc production cross-section with an 18MeV medical pet cyclotron. Appl. Radiat. Isot. 129, 96–102. https://doi.org/10.1016/j.apradiso.2017.08.013.

Carzaniga, T.S., van der Meulen, N.P., Hasler, R., Kottler, C., Peier, P., Turler, A., Vermeulen, E., Vockenhuber, C., Braccini, S., 2019. Measurement of the 43Sc production cross-section with a deuteron beam. Appl. Radiat. Isot. 145, 205–208. https://doi.org/10.1016/j.apradiso.2018.12.031.

Chen, J., Singh, B., Cameron, J.A., 2011. Nucl. Data Sheets 112, 2357. https://doi.org/10.1016/j.nds.2011.08.005.

Mccutchan, E., 2012. Nucl. Data Sheets 113, 1735. https://doi.org/10.1016/j.nds.2012.06.002.

Nelson, A.D., Clark, A.M., Bailey, T.L., Callahan, L.K., Collon, P., 2022. A novel activation technique for integrated cross section measurements using accelerator mass spectrometry. Nucl. Instrum. Methods Phys. Res. Sect. B Beam Interact. Mater. Atoms 533, 50–55. https://doi.org/10.1016/j.nimb.2022.10.016.

Otuka, N., et al., 2014. Towards a more complete and accurate experimental nuclear reaction data library (EXFOR): international collaboration between nuclear reaction data centres (NRDC). Nucl. Data Sheets 120, 272–276. https://doi.org/10.1016/j.nds.2014.07.065.

Severin, G., Engle, J., Valdovinos, H., Barnhart, T., Nickles, R., 2012. Cyclotron produced 44gSc from natural calcium. Appl. Radiat. Isot. 70, 1526–1530. https://doi.org/10.1016/j.apradiso.2012.04.030.

Singh, B., Chen, J., 2015. Nucl. Data Sheets 126, 1. https://doi.org/10.1016/j.nds.2015.05.001.

Sitarz, M., Szkliniarz, K., Jastrzebski, J., Choinski, J., Guertin, A., Haddad, F., Jakubowski, A., Kapinos, K., Kisieli nski, M., Majkowska, A., Nigron, E., Rostampour, M., Stolarz, A., Trzcinska, A., Walczak, R., Wojtkowska, J., Zipper, W., Bilewicz, A., 2018. Production of Sc medical radioisotopes with proton and deuteron beams. Appl. Radiat. Isot. 142, 104–112. https://doi.org/10.1016/j.apradiso.2018.09.025.

Szkliniarz, K., Sitarz, M., Walczak, R., Jastrzebski, J., Bilewicz, A., Choinski, J., Jakubowski, A., Majkowska, A., Stolarz, A., Trzcinska, A., Zipper, W., 2016. Production of medical Sc radioisotopes with an alpha particle beam. Appl. Radiat. Isot. 118, 182–189. https://doi.org/10.1016/j.apradiso.2016.07.001.

Tilley, Weller, Cheves, Chasteler, 1995. Energy levels of light nuclei A=18-19. Nucl. Phys. 595, 1. https://doi.org/10.1016/0375-9474(95)00338-1.

Vakilova, G., Vasidov, A., Mukhammedov, S., Pardaev, E., Rakhmanov, A., Saidmuradov, Zh, 1983. Sensitivity of the determination of some elements with $Z \leq 42$ by a deuteron activational method in a cyclotron. At. Energ. 55, 164. https://doi.org/10.1007/BF01127995.

Zerkin, V.V., Pritychenko, B., 2018. The experimental nuclear reaction data (EXFOR): extended computer database and retrieval system. Nucl. Instrum. Methods Phys. Res. Sect. A Accel. Spectrom. Detect. Assoc. Equip. 888, 31–43. https://doi.org/10.1016/j.nima.2018.01.045.

Ziegler, J., Biersack, J., 2010. The stopping and range of ions in matter. NIM B. https://doi.org/10.1016/j.nimb.2010.02.091.